*

Investigation of AlGaN-Delta–GaN-Based UV Photodiodes in a Metal–Semiconductor–Metal Configuration for Efficient and Fast Solar Blind UV Sensing

Solumtochukwu F. Nwabunwanne, Bryan Melanson, Jing Zhang, and William R. Donaldson

***Abstract*— Metal–semiconductor–metal (MSM) configured UV photodiodes (PD's) were designed and fabricated on an AlGaN/GaN–based substrate for efficient and ultrafast UV detection. The purpose was to investigate the feasibility of obtaining efficient and ultrafast temporal response from these devices in the UV given the challenges associated with the formation of Schottky contacts on laterally oriented AlGaN/GaN thin films. Two sets of devices were implemented using Pt and Au as metal contacts with 5-μm finger width, 5-μm finger spacing, and a 50-μm × 50-μm active area. Spectral and voltage bias studies were done to establish the spectral profile and the effect of bias voltage on the responsivity of the detectors at 265 nm. The best vertical MSM PD's produced 0.6-A/W responsivity under 10-V bias voltage at 265 nm. Peak spectral responsivities were recorded as 1.35 A/W and 1.25 A/W at 240 nm for Pt and Au PD's, respectively.**

***Index Terms*—AlGaN, GaN, efficient, spectral responsivity, ultrafast, PIN, MSM, UV, photodetector, vertically oriented, PD, Pt, Au.**

I. Introduction

Vertical epitaxial structures of aluminum-gallium-nitride (AlGaN) and gallium nitride (GaN) heterostructures, facilitate fast and efficient sensing of UV light in p-type–intrinsic–n-type (p-i-n) and avalanche configurations. Photodiodes (PD's) manufactured on AlGaN templates possess sharp cutoff edges, making them appropriate in setups that need multiple light sources in close proximity like in space exploration vehicles, plasma diagnostics, and target chambers for fusion experiments [1–4]. AlGaN heterostructures are attractive for UV sensing because they have tunable wide and direct-energy band gaps. GaN alloys can sense optical radiation spanning the entire UV spectrum. Spectral window selectivity is supported by simply changing the percentage of Al in the $Al_xGa_{1-x}N$ (x: 0 to 1) alloy [5–8]. Our group and others have reported that the metal–semiconductor–metal (MSM) configuration gives the fastest possible response for GaN/AlGaN-based PD's since, in this mode, the response time of the detector is carrier transit time limited. The small capacitance due to the narrow-interdigitated fingers translates to ~1-ps resistor-capacitor time constant when terminated by a 50-Ω electrical load [9]. The ~1-ps time constant is usually ignored given that the carrier transit time is significantly greater than 1 ps in practice.

In this article, we report the successful design, implementation, and characterization of a novel class of AlGaN/GaN-based UV detectors. These new PD's harness the ultrafast capabilities of the MSM configuration and the robust quantum efficiency of p-i-n quantum wells (QW's). To the best of the authors' knowledge, MSM-configured vertical epistacked GaN/AlGaN-based UV photodetectors have not been reported previously in literature. The objective of this research was to experimentally demonstrate the feasibility of obtaining ultrafast and efficient response from MSM PD's fabricated on p-i-n structured GaN/AlGaN templates under UV radiation. For this study, we employed the delta-GaN QW deep UV wafer configuration [10] shown in Fig. 1. Currently, monolithic integration of lasers/light-emitting diodes (LED's), modulators, and PD's are of immense applicability in optical communication systems and optical interconnect schemes [11–13]. Therefore, we have decided on utilizing the AlGaN-delta-GaN MQW epistructure for our UV PD in this work. Devices with different metal contacts yielded distinct temporal response

*Submitted 11 November 2022. Solumtochukwu F. Nwabunwanne is with Plasma and Ultrafast, Laser Science and Engineering Division, Laboratory for Laser Energetics, University of Rochester, Rochester, NY 14623 USA (e mail: solumtochukwu.nwabunwanne@rochester.edu).

This material is based upon work supported by the Department of Energy National Nuclear Security administration under Award Number DE-NA0003856, the University of Rochester, and the New York State Energy Research and Development Authority. Additional support was supplied by a DOE SBIR grant to Sydor Technologies, of which the University of Rochester Laboratory for Laser Energetics is a Subcontractor.

Solumtochukwu F. Nwabunwanne and William R. Donaldson are affiliated with Plasma and Ultrafast, Laser Science and Engineering Division, Laboratory for Laser Energetics, and Department of Electrical and Computer Engineering, University of Rochester.

Bryan Melanson and Jing Zhang are with Department of Electrical and Microelectronic Engineering, Rochester Institute of Technology.

parameters. An Au device produced a temporal response of 25.4-ps rise time with 415.8-ps pulse duration, while a Pt device recorded 16.6-ps rise time and 253.8-ps pulse width. Also, the responsivities of both Au and Pt devices had different peaks; Au PD peaked at 1.25 A/W [external quantum efficiency (EQE) = 646%] under 240-nm radiation, while Pt PD had a maximum of 1.35 A/W (EQE = 684%) responsivity under 240 nm at 10-V bias. These >1-A/W responsivities indicate that the detectors were in persistent photoconductivity (PPC) mode as a result of the multiplication of charge carriers within the QW, which degraded the response speed of the detectors.

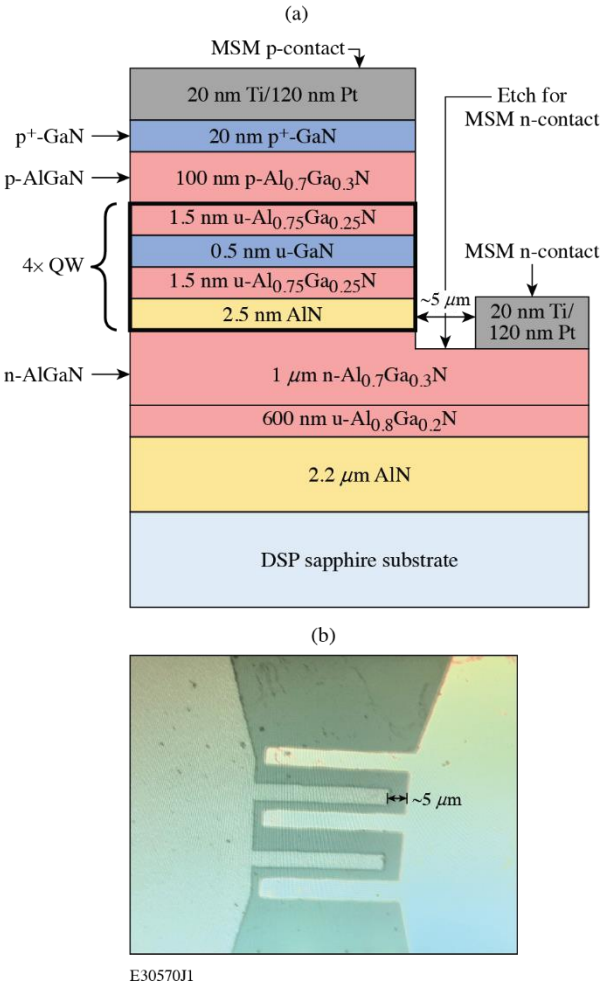

Fig. 1 (a) Epitaxial structure of p-i-n AlGaN/GaN thin films used to fabricate the vertical MSM UV PD's. (b) As-fabricated device showing the 50-μm × 50-μm active area, interdigitated contacts, and compensation pad.

II. Design and Manufacture of the Device

Given the challenges of formation of Schottky contacts and photoconductivity that are associated with laterally oriented AlGaN thin film MSM PD's, it was considered worthwhile to study the feasibility of using a vertically structured p-i-n AlGaN/GaN heterostructure on sapphire to obtain efficient and ultrafast UV photodetection. The customized AlGaN-delta-GaN QW wafer [10] shown in Fig. 1(a) was grown by metal organic chemical vapor deposition (MOCVD). The vertical epitaxial structure of these devices consists of a 2.2-μm AlN nucleation layer grown on a 50.8-mm-diam, 425-μm-thick sapphire wafer, followed by 600 nm of $Al_{0.8}Ga_{0.2}N$, 1 μm n-$Al_{0.7}Ga_{0.3}N$, and four QW stacks consisting of a 2.5-nm AlN barrier layer, an undoped 1.5-nm $Al_{0.75}Ga_{0.25}N$ bottom sub-QW layer, an undoped 0.50-nm GaN delta-layer, and an undoped 1.5-nm $Al_{0.75}Ga_{0.25}N$ top sub-QW. The quantum wells are capped by a 100-nm-thick p-$Al_{0.7}Ga_{0.3}N$ layer and a 20-nm-thick p+-GaN contact layer. Figure 1(b) portrays the as-fabricated device. The energy band diagram of the MSM configured p-i-n AlGaN/GaN UV PD under applied bias voltage and illumination is illustrated in Fig. 2.

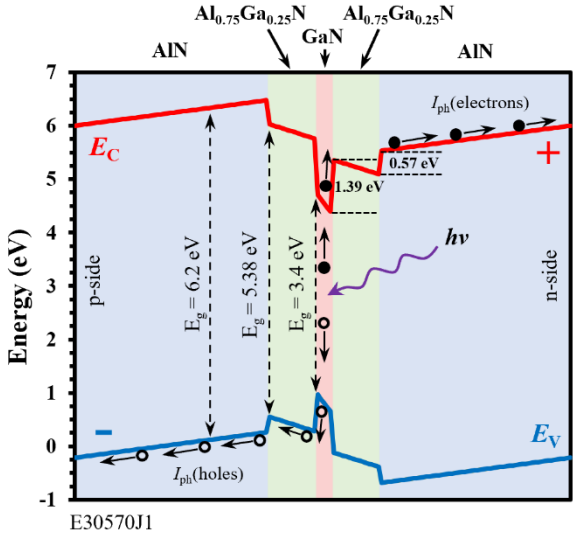

Fig. 2 Simplified (showing only a single quantum well) energy band diagram of AlGaN-delta-GaN QW UV PD under bias and illumination conditions.

Incident UV light illuminates the device from the top and through the sidewalls of the etched mesas, inducing photogeneration of carriers (as illustrated in Fig. 2), which is a function of the incident light's intensity, material quality, and optical characteristics of the absorbing semiconductor thin film. This particular vertical configuration was optimized for an LED application to enable us to share a foundry fabrication run with another project. Figure 3 shows the simulated photoluminescence of this customized wafer with peak at 259 nm.

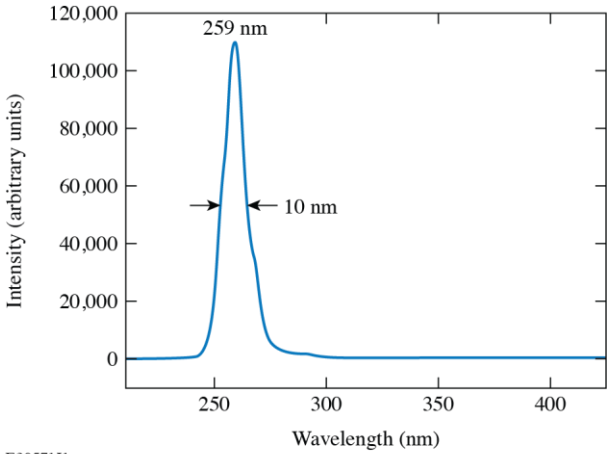

Fig. 3 Simulated photoluminescence (PL) of the epitaxial structure of the p-i-n AlGaN/GaN thin films (peaked at 259 nm with 10-nm FWHM) used to fabricate the vertical MSM UV PD's.

Fabrication of these PD's involved standard photolithography, physical vapor deposition, and plasma etching. Two categories of devices were designed, fabricated, and tested; one set of devices had Pt contacts and the other category had Au contacts.

The MSM structured devices on vertical oriented AlGaN/GaN heterostructure were fabricated at the Integrated Nanosystems Center (URnano) at the University of Rochester and Semiconductor & Microsystems Fabrication Laboratory of the Rochester Institute of Technology. Design files were created using the Clewin5 [14] application and then converted into laser draw files for execution by the laser writer. Positive KL6003 photoresist was employed for photolithography.

Pt and Au were used as metal contacts because they form good Schottky contacts on AlGaN/GaN thin films. This is because they possess high work functions, which improves the rectification properties of MSM PD's fabricated with them. Another motivation for using Pt and Au was for consistency with our previous MSM PD's that were grown on lateral AlGaN/GaN thin films for direct comparison of their performance [8,15]. Finally, Au and Pt were employed to show that although Schottky contacts were formed at both p and n layers, the QW's dominated the diode's rectification property of the devices. This is evident in the asymmetry in the new MSM p-i-n PD's IV curve in Fig 5. Both metal contact types had 20 nm Ti as an adhesion layer with either 120 nm Pt or 120 nm Au as contact metals. Pt was evaporated via e-beam technology, while Au was deposited using thermal evaporation. For n contact metallization, 300 nm was etched into the thin film to expose the n-AlGaN layer using 32 sccm of Cl_2, 8 sccm of BCl_3, and 5 sccm of Ar at 75-W radio-frequency power and ran for 60 s. Figure 1(b) shows a top view of the device design that was fabricated, having a 50-μm × 50-μm active area, a total of five interdigitated electrodes of 5-μm finger width, and 5-μm finger spacing.

Prior to fabrication, x-ray diffraction measurements were conducted to ascertain the dislocation density of defects within the thin films since these material defects are linked with elevated dark currents and poor device performance. Five points were chosen at random within the 2-in. wafer for the rocking curve investigation. The outcomes of the x-ray rocking curve measurements are depicted in Fig. 4. The Hirsch model expressed in Eq. (1) was used to calculate the dislocation density form the x-ray diffraction measurement [16]

$$\rho = \beta^2 / 9\mathbf{B}^2 , \qquad (1)$$

where $\beta = 0.5H \times \sqrt{(\pi/\log_e 2)}$, β is the rocking curve broadening in radians, ρ = the dislocation density, **B** denotes Burger's vector (which is a vector that models the magnitude and phase of the lattice distortion due to crystal lattice dislocation), and H = the rocking curve's FWHM (116.12 arcsecs). The peaks refer to sapphire and the $Al_xGa_{1-x}N$ thin films. The dislocation density was calculated as 3.7119×10^7 cm^{-2}, which indicates that while the material is of good quality with respect to reported GaN/AlGaN material properties [17–19], there are significant numbers of defect sites within the thin films. It is estimated that the number of defects within each detector is approximately 925 given that the detector's active area is 50 μm × 50 μm.

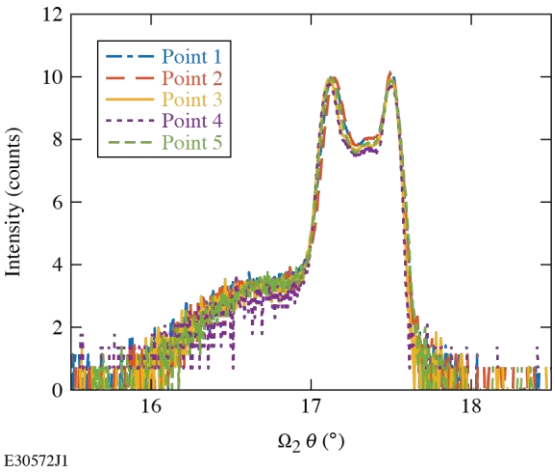

Fig. 4. P-i-n AlGaN/GaN thin film x-ray rocking curves along 002 direction at five different points on the thin film.

The current-voltage (IV) characteristics of one of the MSM-configured p-i-n AlGaN/GaN-based UV detectors under dark conditions is illustrated in Fig. 5. From the simulated energy band diagram depicted in Fig. 2, we see that the elevated series resistance of this PD is attributed to the total 1.96-eV effective barrier height from the AlGaN-delta-GaN/AlN QW. The maximum current obtained in forward-bias mode is 8.2 μA at 20 V and 9.88 μA in reverse-bias mode at -20 V. Also shown in Fig. 5 is the difference between the forward and reverse bias current with respect to the bias voltage. It is apparent that the asymmetry begins when the detector switched on.

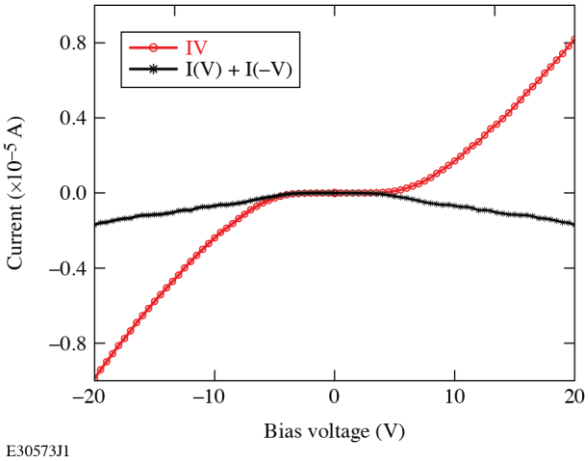

Fig. 5. IV curve of Pt rectangular asymmetric (RA) MSM configured p-i-n AlGaN/GaN UV PD under dark conditions. The asymmetry in the IV is shown by the black curve.

This ~17% difference between forward and reverse bias current of the device suggests that the quantum well, not the Schottky contact, may be the reason for the diode behavior of the device. This is because current is confined within the quantum wells, such that Schottky contacts mainly serve to provide electrical connection with the external circuitry for biasing the device and signal transmission. Also, Schottky diodes require that two metal/semiconductor junctions be arranged back to back, so that the depletion regions overlap, to provide the expected diode rectification. In these devices,

however, there is a vertical separation between the contacts because they were grown on distinct semiconductor layers (n and p regions). This implies that the contacts, via the interdigitated fingers, function to regulate the carrier transit time by creating the shortest practically possible electrical path to the external measurement system. Furthermore, MSM PD's with Schottky contacts exhibit symmetry in their IV curves [8], while some discrepancies may exist in p-i-n diodes due to the complex carrier dynamics with respect to the electric field within the quantum well [20,21]. The variation in the amplitude of the dark current with respect to the bias voltage is attributable to the asymmetric gain in the quantum well multiplication of carriers driven by the polarity of the electric field. Electrons and holes possess different mobilities; therefore, they travel at different speeds as a function of the electric field. At elevated electric fields (as within these detectors), carrier collisions create additional charge carriers via impact ionization, which is the physics behind the gain. The multiplication factor (M) in a two-carrier system is given by Eq. (2) [22]:

$$M = \frac{\alpha_e - \alpha_h}{\alpha_e * e^{-(\alpha_e - \alpha_h)*w} - \alpha_h}, \quad (2)$$

where w is width of the intrinsic region, and α_e and α_h are the electron and hole ionization coefficients, respectively. On the other hand, if the multiplication is only due to the electron, then the ionization ratio (k) specifies the achieved gain and $k = (\alpha_e)/(\alpha_h)$ [22]. While it is possible that both electrons and holes can trigger avalanche multiplication via impact ionization, we are of the opinion that in these devices, electrons are probably responsible given that the carrier mobility of electrons in AlGaN/GaN material system is ~ 127 $cm^2V^{-1}s^{-1}$ [8], which is significantly larger than that of holes which is ~20 $cm^2V^{-1}s^{-1}$ [15]. Hence given the same electric field, electrons will attain avalanche and dominate process. Assuming the avalanche is due to only electrons, we can calculate the ionization ratio (k) for these devices as 9.24 at an electric field of 1×10^7 V/cm, using $\alpha_e = 2.9 \times 10^8 \exp(-3.4 \times 10^7/E)$ [23] and $\alpha_h = 6.8 \times 10^6 \exp(-1.87 \times 10^7/E)$ [23] from the Monte Carlo model. The measured EQE showed a gain factor of 6.

III. Investigations

The same external broadband coupling circuit and experimental setup used to characterize the ultrafast temporal response and external quantum efficiency profiles of the laterally oriented MSM AlGaN PD's given in [15] was employed to test the vertically oriented MSM AlGaN/GaN PD's for ultrafast UV photo-sensing. Figure 6 shows the impulse response functions of Au and Pt MSM configured p-i-n AlGaN-Delta-GaN devices under 20-V bias.

The two devices under test were excited by 265-nm, 30-fs short UV pulses and yielded 25.4-ps, 16.6-ps rise time and 415.8-ps, 253.8-ps FWHM, respectively. There is a considerable tail that extends beyond 2 ns after excitation for the Au device.

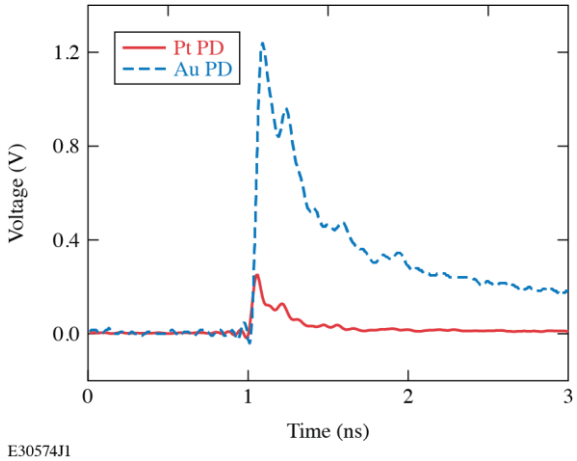

Fig. 6. Au and Pt devices with 25.4-ps, 16.6-ps rise time and 415.8-ps, 253.8-ps pulse width, respectively.

There is a second peak in both response functions of the Au and Pt MSM-configured p-i-n AlGaN-Delta-GaN devices that occur ~200 ps after the primary photoexcitation peak. The presence of these peaks broadened the effective pulse width (FWHM) of the device even though the individual temporal features remained narrow. These secondary peaks in the response functions are likely due to the presence of the 0.5-nm delta GaN layers within the quantum well. Given that this vertical epi structure was primarily set up for LED's [10], the GaN layer was introduced to enhance the electron–hole wave-function overlap in the quantum well. In the absence of the GaN layer, electron–hole wave functions will drift to opposite sides of the AlGaN QW because of the material's internal polarization fields. This drift will drastically reduce the radiative recombination rate of any LED grown on this epitaxial structure, consequently reducing its efficiency. Therefore, adding the GaN layers will increase the recombination of electron–hole pairs in the AlGaN QW's. Additional carriers can be generated by deep UV excitons [24], produced in the AlGaN sub-QW layers, which recombine and emit photons before being removed from the QW. The longer-wavelength photons are then reabsorbed by the 2-nm GaN layer. These generated carriers are later removed, leading to the secondary peak in the response function. These reabsorbed carriers take approximately 200 ps to acquire sufficient energy from the present high electric field to be re-emitted from the quantum well [25,26]. Hence, eliminating the very thin GaN layer may remove the secondary peak at the cost of reducing the internal quantum efficiency of the detector.

IV. Spectral Voltage Studies Outcomes and Discussions

To determine the effect of bias voltage on the temporal response profile of the MSM p-i-n PD's, rise time and pulse duration were studied as functions of bias voltage from 0 to 20 V under 262-nm illumination. The outcome of this investigation is shown in Fig. 7(a). We see that from 0 to ~2.5 V, there were no significant data since the QW barrier had yet to be overcome. This implies that the carriers' transit time in the QW at this range is greater than the recombination time of the carriers in the QW. Then between 3 V to 20 V, both rise time and pulse duration appeared to have a constant behavior

with mean values of 34 ps and 300 ps, respectively. Figure 7(b) displays the rise time and pulse duration as functions of the incident light's wavelength.

While the rise time appeared to be unaffected by wavelength changes, the pulse duration showed significant variations. This further supports the hypothesis that the secondary peak in the response is because of the 2-nm GaN layer in the intrinsic sub-QW as the pulse duration of the response profile varied with wavelength in Fig. 7(b).

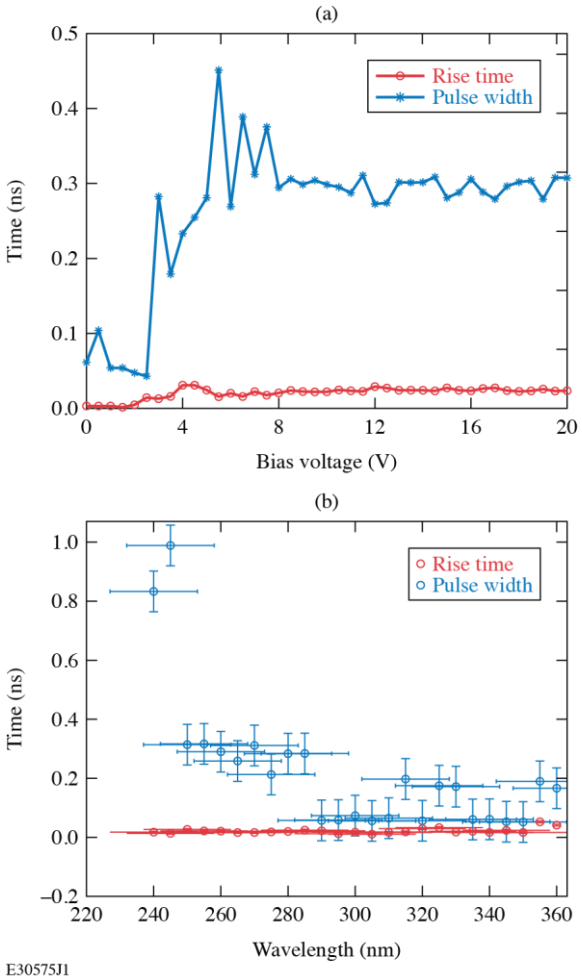

Fig. 7. Typical MSM configured p-i-n AlGaN/GaN PD rise time and pulse duration as functions of (a) bias voltage under 262-nm illumination and (b) wavelength at 10-V bias.

A Lambda 950 photo spectrometer was employed to measure the transmission profile of the p-i-n AlGaN/GaN thin film used to fabricate the devices under review. The data from this measurement listed in Fig. 8 show that cutoff edge of the device is 268 nm (4.64 eV). The additional 20% transmission loss at 300 nm is attributable to variations in the refractive index [$n(\lambda)$] of AlGaN/GaN with respect to input light's wavelength as described by Engelbrecht [27].

The responsivity versus wavelength measurements of Au and Pt devices shown in Fig. 9(b) suggest that there are likely two devices within each PD. This is due to the dual materials used in the absorption layer of the QW. The ~12-nm-thick AlGaN layers in the QW with ~75 % Al are responsible for the first cutoff edge seen at 268 nm, while the ~2-nm-thick GaN layers account for the responsivities from 310 nm to 380 nm in Fig. 9(b). The variations in the responsivities of both Au and Pt devices are likely a result of nonuniformity of material properties within the semiconductor thin films. The differences may also be attributed to the higher work function of Pt that modified the device functional condition at the heterojunction of the metal and semiconductor. This implies that $E_g > h\nu > q\phi_{metal}$ and $V < V_B$ and internal photoemission is operational at different levels within both Au and Pt devices [8,28]. Internal photoemission is a process whereby photoexcited electrons in the metal contact possess sufficient energy to be reabsorbed by the PD's absorption region [28]:

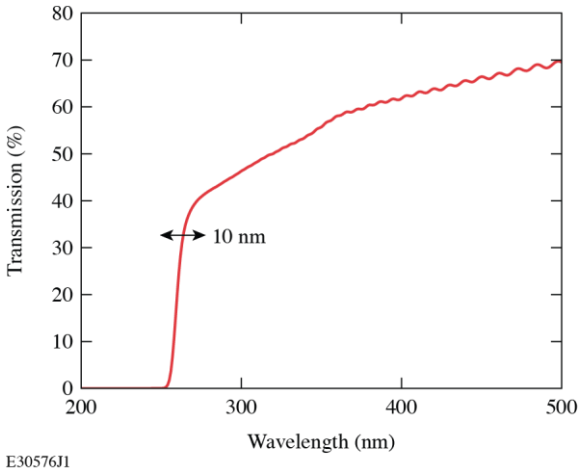

Fig. 8. Transmission profile of p-i-n AlGaN/GaN thin film with 10 nm FWHM from PL data highlighted by the blue arrow.

$$R = \frac{I_{ph}}{P} = \frac{I_{illumination} - I_{dark}}{P}, \qquad 3)$$

where I_{ph} (photocurrent) = illumination current – dark current (in amperes) and P is the incident optical power on the detector (in watts).

Equation (3) was used to calculate the responsivity of Au and Pt MSM configured p-i-n AlGaN/GaN detectors versus bias voltage and wavelength, with the outcomes plotted in Figs. 8(a) and 8(b), respectively. From Fig. 9(a), both devices exhibited their peak responsivities at 19.5 V with the Pt PD having 0.2 A/W and the Au PD showing 1.2 A/W at 8.19-μA dark current. The Au PD yielded higher responsivity as a function of bias voltage because of the significant larger effect of the PPC effect observed in its temporal response function plotted in Fig. 6. The differences in the levels of the observed PPC in Au and Pt device is attributable to the variation in the number of defects within each device because the defect density varied across the 2-in. wafer by ~17% from the x-ray diffraction measurements. This indicates that the Au device was grown on a section of the wafer with more defects, creating more trap sites in the Au device, which led to the noisier and longer pulse duration of 415.8 ps, unlike Pt device that exhibited 253.8-ps pulse duration. Another plausible explanation for the pronounced PPC is the difference in the surface chemistry at both Au and Pt devices' metal/semiconductor interface, leading to different number of interface states, which translated to greater PPC in Au PD than in Pt device. The linear relation between responsivity and bias suggest that the device has yet to attain saturation. The spectral responsivity profiles of both

devices are shown in Fig. 9(b), indicating the 10-nm cutoff edge shown in Fig. 2 and Fig. 7. Here the Pt device exhibited a maximum responsivity of 1.35 A/W at 240 nm with a sharp cutoff at 260 nm. On the other hand, the Au device peaked with 1.25 A/W at 240 nm with a cutoff at 265 nm. This 5-nm difference in the cutoff edges of both devices may be attributable to the ~0.46-eV difference in Pt and Au Schottky barrier heights. At 260 nm, a 5-nm difference accounts for a 0.09-eV change in photon energy. While the energy bandgap of the AlGaN PD's absorption layer drives the cutoff wavelength of the device [29], other factors such as the effective barrier height at the metal/semiconductor heterojunction determined by the Schottky contacts and doping profile can modify the bandgap, facilitating internal photoemission [28,29]. The difference between Pt and Au work functions implies unequal Schottky barrier heights and different levels of internal photoemission process in both devices, leading to the observed ~5-nm (~248-eV) variation in their cutoff edges. Next, since Pt has a greater lattice mismatch than Au, we expect more surface states with Pt devices than with Au devices [30].

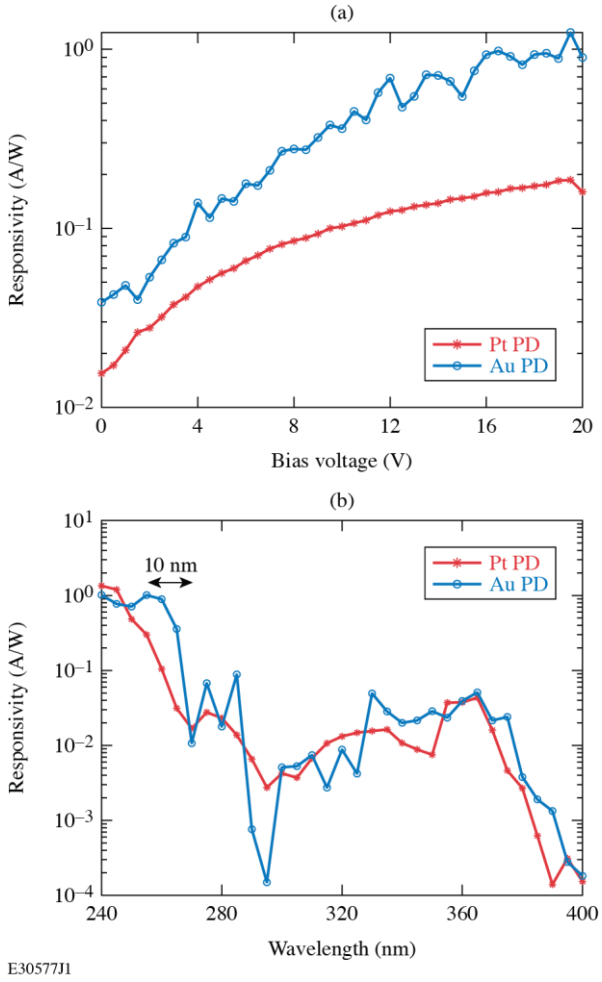

Fig. 9. Responsivity as a function of (a) bias voltage at 262-nm illumination and (b) wavelength under 10 V for Au and Pt devices. The blue arrow indicates the 10 nm FWHM.

In these photodetectors, Schottky and QW confinement are the two physical mechanisms that can provide the observed diode characteristics, but the QW carrier transport mechanism dominated given the asymmetry in the IV curve shown in Fig. 5. Schottky barriers provide the rectification property in MSM PD's by blocking the current below the barrier threshold. Schottky barrier and the p–n junction formed in the QW of these MSM-configured p-i-n AlGaN/GaN UV PD's serve to confine photogenerated carriers in the multiple quantum wells (MQW's) for improved sensitivity. The photocurrent is enhanced by the carrier generation process between electrons produced via avalanche multiplication and tunneling in the QW and holes injected from P+ –GaN/P-AlGaN heterojunction at elevated e-fields [31]. As the bias voltage increased, the Fermi level of GaN rises above the AlGaN's conduction band, facilitating tunneling of electrons into the conduction band [31]. These additional electrons produced in the MQW are promptly removed at the metal contacts by the high electric field before they can recombine with the slower holes injected from P+ -GaN/P-AlGaN interface. This accounts for the improved sensitivity and the secondary peak in the temporal response.

Polarization-assisted electric field enhances the photocurrent generation in AlGaN/GaN-based UV PD's by increasing the penetration of the electric field and absorption of UV photons in polarization-assisted UV PD designs [32]. However, polarization did not affect the PD's reported in this study since the electric field is perpendicular to the 2-D QW's.

The data in Fig. 10 is from the Au p-i-n AlGaN/GaN device at 351-nm UV illumination under 20-V bias and a conventional MSM AlGaN PD, which was illuminated by a 262-nm UV light, yielding a 32-ps rise time and 62-ps FWHM. At 351 nm, the AlGaN layers of the QW in the Au p-i-n AlGaN/GaN device should be transparent and non-absorbing; the absorption will occur only in the GaN layers. The carrier recycling mechanism discussed above can still operate. These data suggest that it is possible to obtain ultrafast response using the MSM configuration on a p-i-n AlGaN/GaN structure, but it will require optimization of the QW design to yield a single peak. This will be the subject of a future publication. Hence,

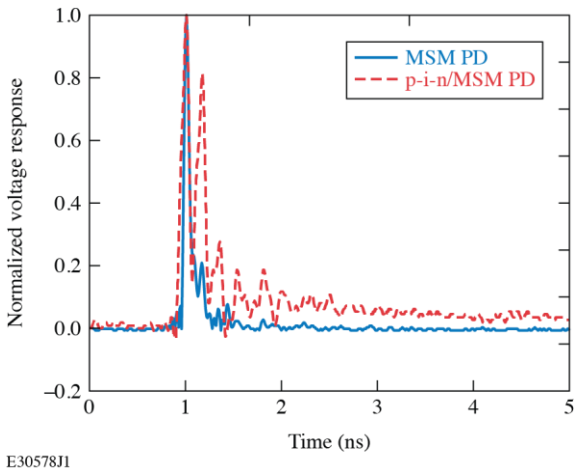

Fig. 10. Temporal response of Au p-i-n AlGaN/GaN device at 351-nm UV excitation under 20-V bias with 39.2-ps rise time, 121.7-ps pulse duration, and a conventional lateral MSM PD under 262-nm illumination and 20-V bias, with 32-ps rise time, 62-ps pulse duration.

obtaining a single peak from the next-generation p-i-n AlGaN/GaN devices should yield a response time that is approximately equal to the pulse duration of the first peak of the Au p-i-n AlGaN/GaN device in Fig. 10, which is 75 ps. For comparison, the conventional MSM PD's response time is 62 ps. Therefore, the p-i-n structure appears to have only slightly degraded the pulse width, but it should remain viable for many of the target applications. The narrow 2 µm spacing between the interdigitated electrodes is responsible for the ultrafast temporal response of the PDs. This narrow spacing lowers the carrier transit path from the QW to the external broadband circuit to < 3 µm. This allows these novel AlGaN/GaN MSM PDs to benefit both from the ultrafast temporal response of MSM devices as well as the efficient sensing of a p-i-n device.

Table 1 compares the results we obtained from these new devices with others reported in literature. While they are not the most sensitive among the listed works, the new devices exhibited superior temporal characteristics as well as satisfactory sensitivity.

Table 1: Comparison of the new devices' temporal response parameters and sensitivity with existing works in literature.

Serial Number	Detector type	Material	Rise time	Pulse width	Responsivity (A/W)	Ref.
1	MSM	GaN	0.862 s	0.981s	13.56	[32]
2	Phototransistor	p-GaN/AlGaN/ GaN/Si	0.41 s	0.77 s	3.5×10^5	[6]
3	MSM	GaN	0.062 s	0.437 s	0.1	[18]
4	Phototransistor	AlGaN	4.4 μs	595.4 μs	5.8×10^3	[33]
5	MSM	GaN	2 ms	5.6 ms	33.3	[34]
6	p-i-n	GaN	–	–	0.2	[35]
7	MSM/p-i-n	AlGaN/Delta/ GaN	16.6 ps	253.8 ps	1.35	This work

V. Conclusion

In summary, we have successfully demonstrated the feasibility of obtaining efficient and ultrafast UV photodetection with MSM-configured vertically oriented AlGaN/GaN-based UV PD's. Voltage studies showed that the devices had a linear responsivity profile with bias voltage from 3.5 V to 15.5 V for an Au device, while the Pt device showed linearity from 3.5 V to 19.5 V. This implies that saturation was imminent in the Au device from 15.5 V. The spectral responsivity of Pt and Au devices are comparable at 1.35 A/W at 240 nm with a sharp cutoff at 260 nm and 1.25 A/W at 240 nm with a cutoff at 265 nm, respectively. Finally, the temporal response of both devices showed that Pt devices had better temporal characteristics with 16.6-ps rise time and 253.8-ps pulse duration, while Au devices had a 25.4-ps rise time and 415.8-ps pulse width due to its long decay tail. These interesting outcomes will provide an alternative path to Schottky contact formation challenges in achieving efficient and ultrafast photosensing in the UV region. It is intended that these novel devices will forge a paradigm shift in the way AlGaN/GaN-based MSM PD's are designed for the high-energy-density physics and the plasma diagnostics communities.

References

1. R. Young, C. C. Kuranz, D. H. Froula, J. Ross, and S. Klein, "Observation of stagnation in counter-streaming laser-created plasmas with optical Thomson scattering," *Bull. Am. Phys. Soc.*, vol. 63, no. 11, 2018, Art. no. BAPS.2018.DPP.GO2014.2011.
2. A. M. Hansen *et al.*, "Cross-beam energy transfer platform development on OMEGA," Bull. Am. Phys. Soc., vol. 63, no. 11, Jan. 2018, Art. no. BAPS.2018.DPP.CO2014.2017.
3. A. M. Saunders *et al.*, "Characterizing plasma conditions in radiatively heated solid-density samples with x-ray Thomson scattering," *Phys. Rev. E*, vol. 98, no. 6, Dec. 2018, Art. no. 063206, doi: https://doi.org/10.1103/PhysRevE.98.063206.
4. B. E. Kruschwitz *et al.*, "Tunable UV upgrade on OMEGA EP," *Proc. SPIE*, vol. 10898, Mar. 2019, Art. no. 1089804, doi: https://doi.org/10.1117/12.2505419.
5. E. Monroy, F. Calle, E. Muñoz, and F. Omnès, "AlGaN metal–semiconductor–metal photodiodes," *Appl. Phys. Lett.*, vol. 74, no. 22, pp. 3401–3403, May 1999, doi: https://doi.org/10.1063/1.123358.
6. Q. Lyu, H. Jiang, and K. M. Lau, "Monolithic integration of ultraviolet light emitting diodes and photodetectors on a p-GaN/AlGaN/GaN/Si platform," *Opt. Express*, vol. 29, no. 6, pp. 8358–8364, Mar. 2021, doi: https://doi.org/10.1364/OE.418843.
7. M. Gökkavas, S. Butun, T. Tut, N. Biyikli, and E. Ozbay, "AlGaN-based high-performance metal–semiconductor–metal photodetectors," *Photonic Nanostruct.*, vol. 5, no. 2, pp. 53–62, Oct. 2007, doi: https://doi.org/10.1016/j.photonics.2007.06.002.
8. S. F. Nwabunwanne and W. R. Donaldson, "Boosting the external quantum efficiency of AlGaN-based metal–semiconductor–metal ultraviolet photodiodes by electrode geometry variation," *IEEE J. Quantum Electron.*, vol. 57, no. 6, Art. no. 4000608, Dec. 2021, doi: https://doi.org/10.1109/JQE.2021.3117953.
9. Y. Zhao and W. R. Donaldson, "Ultrafast UV AlGaN metal–semiconductor–metal photodetector with a response time below 25 ps," *IEEE J. Quantum Electron.*, vol. 56, no. 3, Jun. 2020, Art. no. 4000607, doi: https://doi.org/10.1109/JQE.2020.2981043.
10. C. Liu *et al.*, "234 nm and 246 nm AlN-Delta-GaN quantum well deep ultraviolet light-emitting diodes," *Appl. Phys. Lett.*, vol. 112, no. 1, Dec. 2018, Art. no. 011101, doi: https://doi.org/10.1063/1.5007835.
11. J. Pereiro *et al.*, "Optimization of InGaN–GaN MQW photodetector structures for high-responsivity performance," *IEEE J. Quantum Electron.*, vol. 45, no. 6, pp. 617–622, Jun. 2009, doi: 10.1109/JQE.2009.2013140.
12. M. Feng *et al.*, "On-chip integration of GaN-based laser, modulator, and photodetector grown on Si," *IEEE J. Sel. Top. Quantum Electron.*, vol. 24, no. 6, pp. 1–5, Nov. 2018, doi: 10.1109/JSTQE.2018.2815906.
13. Q. Lyu, H. Jiang, and K. M. Lau, "Monolithic integration of ultraviolet light emitting diodes and photodetectors on a p-GaN/AlGaN/GaN/Si platform," *Opt. Express*, vol. 29, no. 6, pp. 8358–8364, Mar. 2021, doi: 10.1364/OE.418843.

14. "Clewin 5, regular 5-seat commercial license–wieweb software," Accessed 20 April 2021, https://wieweb.com/site/product-category/clewin-software/.
15. S. Nwabunwanne and W. Donaldson, "Interdigitated electrode geometry variation and external quantum efficiency of GaN/AlGaN-based metal-semiconductor-metal UV photodetectors," *Proc. SPIE*, vol. 12001, Mar. 2022, Art. no. 120010F, doi: https://doi.org/10.1117/12.2608355.
16. P. Gay, P. B. Hirsch, and A. Kelly, "The estimation of dislocation densities in metals from x-ray data," *Acta Metall.*, vol. 1, no. 3, pp. 315–319, May 1953, doi: 10.1016/0001-6160(53)90106-0.
17. R. Gaska *et al.*, "Electron transport in AlGaN–GaN heterostructures grown on 6H–SiC substrates," *Appl. Phys. Lett.*, vol. 72, no. 6, pp. 707–709, Feb. 1998, doi: https://doi.org/10.1063/1.120852.
18. A. Chatterjee *et al.*, "Role of threading dislocations and point defects in the performance of GaN-based metal-semiconductor-metal ultraviolet photodetectors," *Superlattices Microstruct.*, vol. 148, Dec. 2020, Art. no. 106733, doi: https://doi.org/10.1016/j.spmi.2020.106733.
19. Y. Zhao and W. R. Donaldson, "Systematic study on aluminum composition nonuniformity in aluminum gallium nitride metal–semiconductor–metal photodetectors," *IEEE Trans. Electron Devices*, vol. 65, no. 10, pp. 4441–4447, Oct. 2018, doi: https://doi.org/10.1109/TED.2018.2862901.
20. Z. Zhang *et al.*, "AlGaN solar-blind p-i-n-i-n APDs employing a charge layer with modulated doping and bandgap," in *Asia Communications and Photonics Conference (ACPC) 2019*, OSA Technical Digest, Chengdu: Optica Publishing Group, 2019, p. M4A.303.
21. N. Biyikli, I. Kimukin, O. Aytur, and E. Ozbay, "Solar-blind AlGaN-based p-i-n photodiodes with low dark current and high detectivity," *IEEE Photonics Technol. Lett.*, vol. 16, no. 7, pp. 1718–1720, Jul. 2004, doi: https://doi.org/10.1109/LPT.2004.829526.
22. L. Chrostowski and M. Hochberg, *Silicon Photonics Design: From Devices to Systems*, 1st ed., Cambridge, England: Cambridge University Press, 2015.
23. L. Cao *et al.*, "Experimental characterization of impact ionization coefficients for electrons and holes in GaN grown on bulk GaN substrates," *Appl. Phys. Lett.*, vol. 112, no. 26, Jun. 2018, Art. no. 262103, doi: https://doi.org/10.1063/1.5031785.
24. J. Yin *et al.*, "Surface plasmon enhanced hot exciton emission in deep UV-emitting AlGaN multiple quantum wells," *Adv. Opt. Mater.*, vol. 2, no. 5, pp. 451–458, Mar. 2014, doi: https://doi.org/10.1002/adom.201300463.
25. I. Sayed and S. M. Bedair, "Quantum well solar cells: Principles, recent progress, and potential," *IEEE J. Photovolt.*, vol. 9, no. 2, pp. 402–423, Mar. 2019, doi: https://doi.org/10.1109/JPHOTOV.2019.2892079.
26. J. A. Brum, T. Weil, J. Nagle, and B. Vinter, "Calculation of carrier capture time of a quantum well in graded-index separate-confinement heterostructures," *Phys. Rev. B*, vol. 34, no. 4, pp. 2381–2384, Aug. 1986, doi: https://doi.org/10.1103/PhysRevB.34.2381.
27. J. A. A. Engelbrecht, B. Sephton, E. Minnaar, and M. C. Wagener, "An alternative method to determine the refractive index of $Al_xGa_{1-x}N$," *Physica B Condens. Matter*, vol. 480, pp. 181–185, Jan. 2016, doi: https://doi.org/10.1016/j.physb.2015.08.047.
28. S. M. Sze, *Semiconductor Devices: Physics and Technology*, 3rd ed., Hoboken, NJ: Wiley, 2012.
29. S. F. Nwabunwanne and W. R. Donaldson, "Demonstration of spectral selectivity of efficient and ultrafast GaN/AlGaN-based metal–semiconductor–metal ultraviolet photodiodes," *IEEE Trans. Electron Devices*, vol. 69, no. 12, pp. 6859–6864, Dec. 2022, doi: https://doi.org/10.1109/TED.2022.3215641.
30. A. Dal Corso, "Clean Ir(111) and Pt(111) electronic surface states: A first-principle fully relativistic investigation," *Surf. Sci.*, vol. 637, pp. 106–115, Jul. 2015, doi: https://doi.org/10.1016/j.susc.2015.03.013.
31. S. Feng *et al.*, "Graphene/p-AlGaN/p-GaN electron tunnelling light emitting diodes with high external quantum efficiency," *Nano Energy*, vol. 60, pp. 836–840, Jun. 2019, doi: https://doi.org/10.1016/j.nanoen.2019.04.007.
32. J. X. Wang *et al.*, "Polarization assisted self-powered GaN-based UV photodetector with high responsivity," *Photonics Res.*, vol. 9, no. 5, pp. 734–740, May 2021, doi: https://doi.org/10.1364/PRJ.418813.
33. K. Wang, X. Qiu, Z. Lv, Z. Song, and H. Jiang, "Ultrahigh detectivity, high-speed and low-dark current algan solar-blind heterojunction field-effect phototransistors realized using dual-float-photogating effect," *Photon. Res.*, vol. 10, no. 1, pp. 111–119, Dec. 2021, doi: https://doi.org/10.1364/PRJ.444444.
34. R. S. Pokharia *et al.*, "A highly sensitive and robust GaN ultraviolet photodetector fabricated on 150-mm Si (111) wafer," *IEEE Trans. Electron Devices*, vol. 68, no. 6, pp. 2796–2803, Jun. 2021, doi: https://doi.org/10.1109/TED.2021.3073650.
35. P. Dalapati, K. Yamamoto, T. Kubo, T. Egawa, and M. Miyoshi, "Bias-controlled photocurrent generation process in GaN-based ultraviolet p–i–n photodetectors fabricated with a thick Al_2O_3 passivation layer," *Optik*, vol. 245, Nov. 2021, Art. no. 167691, doi: https://doi.org/10.1016/j.ijleo.2021.167691.

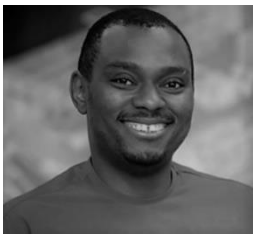

Solumtochukwu F. Nwabunwanne received both his B.Eng. degree in 2007 and M.Eng. degree in 2013 in Electronic Engineering from the Department of Electronic Engineering, University of Nigeria, Nsukka, Nigeria. He received his M.S. degree in Electrical Engineering from the University of Rochester in 2019, where he is currently studying for his Ph.D. degree in Electrical Engineering. He is presently conducting research on ultrafast AlGaN-based UV photodetectors at the Laboratory for Laser Energetics.

Bryan Melanson received his B.S. degree in Materials Science and Engineering with a focus in Nanotechnology and Nanoengineering in 2018 from the University of Washington, Seattle, USA. He joined Dr. Jing Zhang's research group at the Rochester Institute of Technology as a Ph.D. candidate in 2018 and is currently conducting research on deep-ultraviolet light emitting diodes and μLED displays with a focus on improving the light extraction efficiency of these devices.

Jing Zhang is currently the Kate Gleason Associate Professor in the Department of Electrical and Microelectronic Engineering at Rochester Institute of Technology. She obtained her B.S. degree in Electronic Science and Technology from Huazhong University of Science and Technology (2009), and Ph.D. degree in Electrical Engineering from Lehigh University (2013). Dr. Zhang's research focuses on developing highly efficient III-nitride and GaO semiconductor-based photonic, optoelectronic, and electronic devices. Her research group is working on the development of novel quantum well active regions and substrates for enabling high-performance ultraviolet (UV) and visible LED's/lasers, as well as engineering of advanced device concepts for nanoelectronics. Dr. Zhang has published more than 40 refereed journal papers and 70 conference proceedings including invited talks. She is a recipient of Texas Instruments/Douglass Harvey Faculty Development Award, and National Science Foundation (NSF) CAREER Award.

William R. Donaldson (Life Member, IEEE) received the B.S. degree (Hons.) in physics and mathematics from Carnegie Mellon University in 1976 and the Ph.D. degree from the Electrical Engineering Department, Cornell University, in 1984 on the use of organic crystals for an optical parametric oscillator. After graduating in 1984, he joined the Laboratory for Laser Energetics, University of Rochester, as a Research Associate. In 1986, he was promoted to Staff Scientist. In 2009, he was appointed as a professor of Electrical and Computer Engineering with the ECE Department, University of Rochester. His research interests have included the physics of photoconductive switches, streak-camera development, optical response of high-temperature superconductors, optical semiconductor diagnostics, and the florescence of biological molecules. He holds five patents and has published numerous scientific articles. He is a member of the American Physical Society and the Optical Society of America.